remote sensing

Article

CO Emissions Associated with Three Major Earthquakes Occurring in Diverse Tectonic Environments

Yueju Cui, Jianan Huang, Zhaojun Zeng and Zhenyu Zou *

The United Laboratory of High-Pressure Physics and Earthquake Science, Institute of Earthquake Forecasting, China Earthquake Administration, Beijing 100036, China; cuiyueju@ief.ac.cn (Y.C.); canaan0621@163.com (J.H.); zzj00616@163.com (Z.Z.)

* Correspondence: zouzhenyu@ief.ac.cn

Abstract: Significant amounts of gases are emitted from the earth's crust into the atmosphere before, during, and after major earthquakes. To understand the relationship between gas emissions, earthquakes, and tectonics, we conducted a thorough investigation using satellite data from AQUA AIRS. We focused on three major earthquakes: the 12 May 2008 Wenchuan M_W 7.9 earthquake in China's intra-continental plate, the 26 December 2004 Sumatra-Andaman M_W 9.1 earthquake in Indonesia Island, and the 4 April 2010 Baja California M_W 7.2 earthquake in Mexico's active plate margin. Anomalies in the total column (TotCO) and multiple layers (CO VMR) of carbon monoxide were observed along fault zones, with peak values at the epicenter areas. Furthermore, temporal anomalies of TotCO and CO VMR appeared in the month of the Wenchuan earthquake in the intra-continent, three months prior to the Sumatra-Andaman earthquake and one month before the Baja California earthquake in the active plate margins, respectively. Notably, the duration of CO anomalies before earthquakes in active plate margins was longer than that in the intra-continental region, and the intensity of the CO anomaly in active plate margins was higher than that in the intra-continental region. The results show a profound correlation with both seismic and tectonic activities, which was particularly evident in the earthquake's magnitude, rupture length, and the tectonic settings surrounding the epicenter. Furthermore, the type of the fault at which the earthquake occurred also played an important role in these CO anomaly variations. These findings support the identification of earthquake precursors and may help improve our understanding of earthquake forecasting and tectonics.

Keywords: gas emission; earthquake; DTS-V; TotCO; CO VMR

check for updates

Citation: Cui, Y.; Huang, J.; Zeng, Z.; Zou, Z. CO Emissions Associated with Three Major Earthquakes Occurring in Diverse Tectonic Environments. *Remote Sens.* **2024**, *16*, 480. https://doi.org/10.3390/rs16030480

Academic Editors: Pietro Tizzani, Daniele Cirillo and Francesco Brozzetti

Received: 4 January 2024
Revised: 23 January 2024
Accepted: 23 January 2024
Published: 26 January 2024

1. Introduction

Previous research has clearly established that during and after major earthquakes, significant amounts of gases, including Rn, CO_2, CH_4, and CO, are emitted from active fault zones. This has been observed through both ground-based field measurements [1–10] and satellite remote sensing [11–22]. Carbon monoxide, in particular, has been identified as a potential earthquake precursor parameter, as confirmed by numerous case studies using satellite data. Due to its significant presence in the deep crust, it tends to migrate upwards into the atmosphere, following the cracks formed by seismic activity during the earthquake preparation. This observation has been confirmed by numerous case studies using satellite data, further emphasizing the potential role of carbon monoxide as an earthquake precursor. For instance, CO anomalies were observed before, during, and after the 26 January 2001 Gujarat M_S 7.8 Earthquake [13] and the 31 March 2002 Taiwan M_S 7.5 Earthquake [23] using MOPITT data. Other examples include the 26 December 2004 Sumatra 8.9 Earthquake [17], the 5 April 2010 Mexico Baja California M_W 7.2 Earthquake [24], the 12 May 2008 Wenchuan M_S 8.0 Earthquake [15,16], and the 20 April 2013 Lushan M_S 7.0 Earthquake [15,16] using AIRS data, and the 2015 Gorkha (M 7.8) and Dolakha (M 7.3) Nepal earthquakes [19] using MOPITT data. However, the data used in these studies primarily captured the total column of CO, which includes all molecules from the ground to the sensor. This made it challenging to determine the precise layer where the anomaly originated or whether it was truly related to an earthquake or a meteorological phenomenon. This is because meteorological anomalies are predominantly observed in the troposphere, whereas earthquake anomalies typically emanate from closer to the Earth's surface. Therefore, CO profile data were used to investigate CO anomalies in different layers, similar to the air temperature differences reported by Ma et al. [25]. In their study [25], the impacts of multiple layers of air temperature variations on tidal forces and tectonic stress before, during, and after the Jiujiang earthquake were analyzed. By utilizing a similar approach for CO profile data, we aimed to gain further insights into the potential relationship between CO anomalies and seismic activity.

The Chinese Wenchuan M_W 7.9 Earthquake, which occurred on 12 May 2008 with its epicenter located at 31.002°N, 103.322°E (USGS), the Indonesian Sumatra-Andaman M_W 9.1 Earthquake on 26 December 2004 with its epicenter at 3.295°N, 95.982°E, and the Mexican Baja California M_W7.2 Earthquake on 4 April 2010 with its epicenter at 32.286°N, 115.295°W, are three distinct earthquake events that occurred in diverse geographical regions. Each earthquake represented a unique type of seismic activity based on fault mechanics, the depth of rupture, and the geological settings of the affected area. For instance, the Wenchuan Earthquake was characterized by reverse faulting within the tectonically complex Tibetan Plateau, leading to a rupture length of approximately 300 km [26–28]. In contrast, the Sumatra-Andaman Earthquake occurred in a subduction zone offshore of Sumatra, where one tectonic plate slides beneath another, resulting in a much longer rupture of approximately 1200 km [29–31]. Finally, the Baja California Earthquake took place within a dextral strike-slip fault zone on land by the sea, causing a rupture of approximately 75 km [32–34]. The diversity of these earthquake types is significant for our study because it offers an opportunity to investigate how carbon monoxide (CO) emissions vary across different seismic settings. Each earthquake was accompanied by significant emissions of gases from the fault zone, as confirmed through field surveys and satellite data, indicating a potential link between seismic activity and atmospheric gas concentrations. The aim of this study is to investigate the variations in carbon monoxide (CO) levels in both the total column (TotCO) and multiple layers (CO VMR) in relation to these three distinct earthquakes using the method of differences. This will provide valuable insights into the interactions between the lithosphere and atmosphere during seismic activities.

2. Data and Methodology

2.1. Data

The Atmospheric Infrared Sounder (AIRS) was launched onboard the NASA's spacecraft Aqua satellite in May 2002. The AIRS instrument collects a comprehensive dataset, including the CO total column amount (TotCO), CO volume mixing ratios (CO VMR) at 24 altitudes, and the corresponding geolocation fields, which provide latitude, longitude, and pressure level. AIRS CO products were derived with the Singular Value Decomposition (SVD) method using the 4.58~4.50 μm (2183–2220 cm^{-1}) spectrum with the spatial resolution of 45 km and an accuracy of about 15% by pre-launch simulations [35–37]. Level 3 data available as daily, 8-day, and monthly formats are mapped with a resolution of $1.0 \times 1.0°$. For this study, the Version 6 and level 3 standard gridded product of TotCO and CO VMR at 850, 700, 600, 500, 400, 300, and 250 hPa, which are freely available from NASA's Goddard Earth Sciences Data and Information Services Center (http://disc.sci.gsfc.nasa.gov/, accessed on 20 December 2021), was used. To avoid the influence of solar radiation, the study used the descending orbit data.

2.2. Methodology

The abnormal variations based on TotCO and CO VMR were analyzed in this study. The anomalies were derived by the approach described in Equation (1), which calculates the difference between the current gas value and the background fields. Specifically, the anomaly $A(x, y, t, h)$ for a given region is determined by subtracting the background value $G_{bac}(x, y, t, h)$ within a predefined duration spanning 2003 to 2015 from the current gas value $G(x, y, t, h)$. This is expressed mathematically in Equation (1):

$$A(x, y, t, h) = G(x, y, t, h) - G_{bac}(x, y, t, h) \tag{1}$$

$$G_{bac}(x, y, t, h) = \sum_{i=1}^{N} G_i(x, y, t, h)/N \tag{2}$$

where $G(x, y, t, h)$ represents the current gas value, while $G_{bac}(x, y, t, h)$ denotes the computed mean derived from the background field, which is defined as a monthly mean value of gas $G(x, y, t, h)$ over an area with x–y coordinates at the corresponding altitude for the t month at the h layer of N years. For this study, N was set as 13, for the years from 2003 to 2015.

The determination of an earthquake-related anomaly was based on the criterion of DTS-V (Deviation Time Space-Vertical) [25,38,39]. This criterion encompasses four key aspects: (1) deviation, referring to the magnitude of an anomaly's departure from the background; (2) time, which considers the quasi synchronous occurrence of anomalies across multiple parameters; (3) space, influenced by both seismic and tectonic activities, with anomalous regions typically clustering around the epicenter or adjacent fault zones; and (4) vertical, emphasizing the continuity of anomalies' vertical variations. The DTS-V criterion is an advancement that incorporates vertical variations, building upon the foundation of the DTS criterion [38], which was initially utilized for the detection of earthquake-related thermal anomalies [25,39]. More specifically, we assessed whether an anomaly was related to an earthquake by examining its abnormal amplitude, the time when it occurred, and the spatial and vertical distribution of the anomaly.

3. Results

3.1. CO Variations Associated with Wenchuan M_S 8.0 Earthquake

The temporal, spatial, and vertical variations in CO anomalies associated with the Wenchuan Earthquake were analyzed based on the monthly TotCO, monthly CO VMR, and 8-day CO VMR data.

The temporal and spatial variations in monthly TotCO anomaly and CO VMR at different altitudes (850 to 250 hPa) associated with Wenchuan Earthquake are shown in Figures 1 and 2, respectively. The findings revealed that TotCO anomalies occurred near the epicenter area in the month of Wenchuan Earthquake. Furthermore, CO VMR values were detected in the epicenter area and across all layers in May, coinciding with the occurrence of the earthquake [15]. As the AIRS sensor is more sensitive in the troposphere, CO anomalies were more pronounced at altitudes ranging from 300–600 hPa compared to the near-surface levels. Nevertheless, subtle CO anomalies were still detectable near the surface. The elevated values observed in the southeast corner of the figure lack any distinct structural characteristics and are situated significantly distant from the epicenter. This indicates that they are unrelated to the earthquake event and that their occurrence may potentially be attributed to meteorological conditions or other unrelated factors.

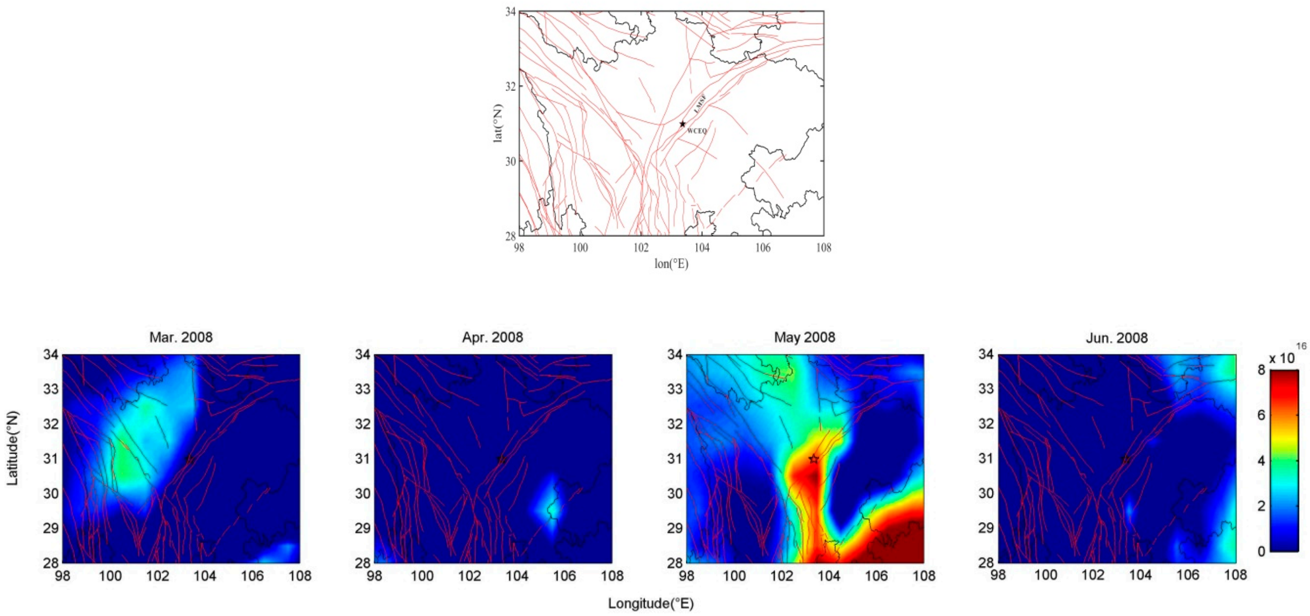

Figure 1. The temporal and spatial variations in TotCO anomaly from March to June 2008 associated with Wenchuan M_W 7.9 Earthquake. A clean base map with only the epicenter and faults were drawn in order to clearly display the location of the epicenter and faults (the upper figure). The red lines represent the faults and black star pinpoints the epicenter (as in Figures 2 and 3). LMSF refers to Longmenshan Fault and WCEQ stands for Wenchuan Earthquake.

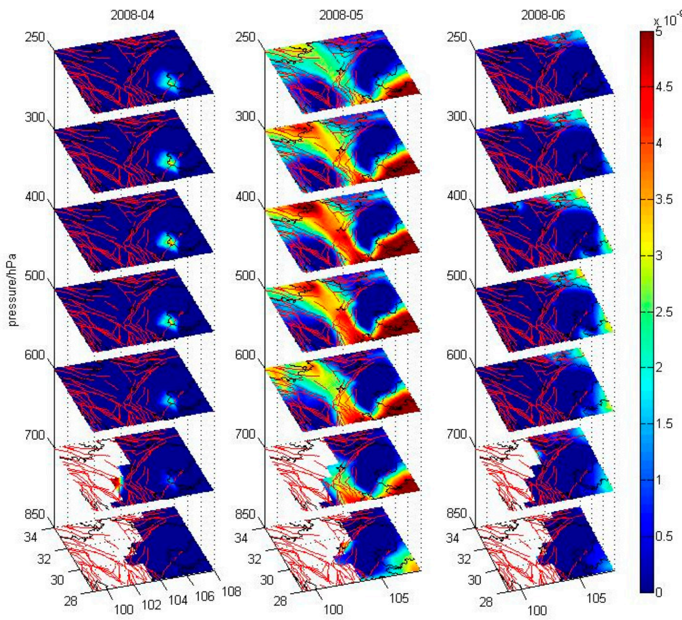

Figure 2. The spatial–vertical variations of CO VMR anomalies in monthly data from April to June 2008 associated with Wenchuan M_W 7.9 Earthquake. White areas at 850 and 700 hPa indicate a lack of data acquisition due to the presence of the Tibetan Plateau, characterized by the low atmospheric pressure and high altitude, located to the west of the Longmenshan Fault (LMSF).

The spatial–vertical variations in CO VMR in 8-day data are displayed in Figure 3. This showed that CO anomalies appeared from 4 May to 20 May 2008, located at the epicenter at 850 and 700 hPa on 4 May, and were distributed along the faults at 700 to 300 hPa on 12 May. By 20 May, the anomalies were concentrated at the epicenter at 600 to 250 hPa. All the phenomena above strongly suggested that these CO anomalies were closely related to the Wenchuan Earthquake, indicating that the CO anomaly apparent in Figures 1–3 originated from the near-surface sources [15].

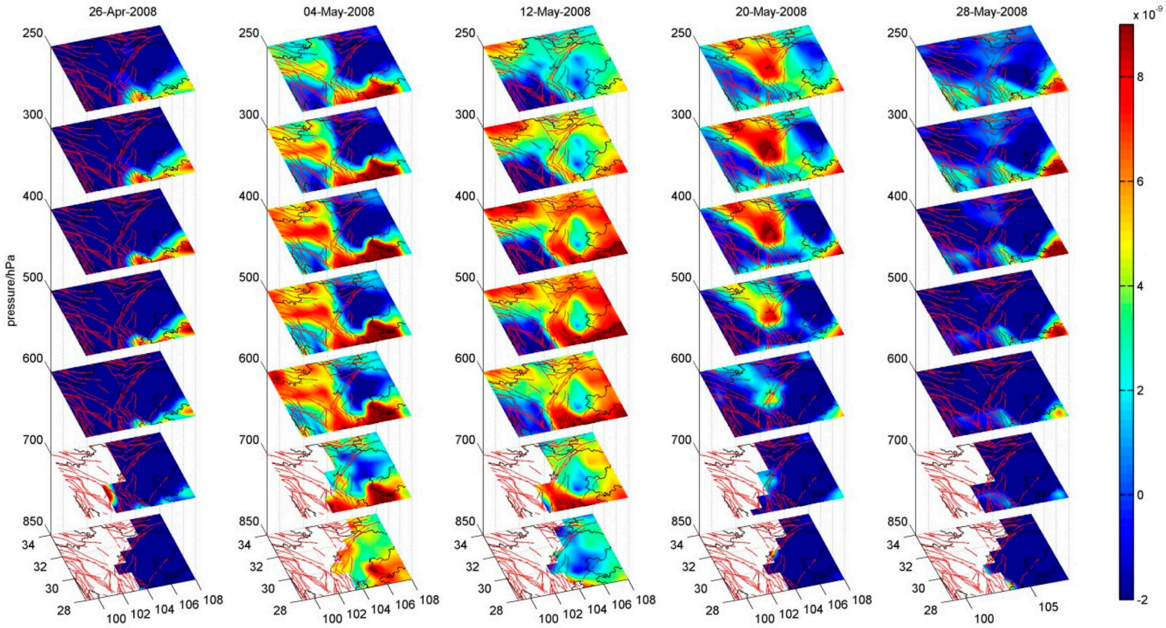

Figure 3. The spatial–vertical variations of CO VMR anomalies in 8-day data from 26 April to 28 May 2008 associated with Wenchuan M_W 7.9 Earthquake.

3.2. CO Variations Associated with Sumatra-Andaman M_W 9.1 and Sumatra-Nias M_W 8.6 Earthquakes

The temporal, spatial, and vertical variations in CO anomalies associated with the Sumatra-Andaman Earthquake were analyzed based on monthly TotCO, monthly CO VMR, and 8-day CO VMR data.

The temporal and spatial variations of TotCO anomaly are shown in Figure 4, spanning from July 2004 to June 2005. Notably, the TotCO anomaly appeared in the vicinity of the epicenter area as early as September 2004, three months before the Sumatra-Andaman M_W 9.1 Earthquake, and persisted until April 2005, even one month after the occurrence of the Sumatra-Nias M_W 8.6 earthquake on 28 March 2005.

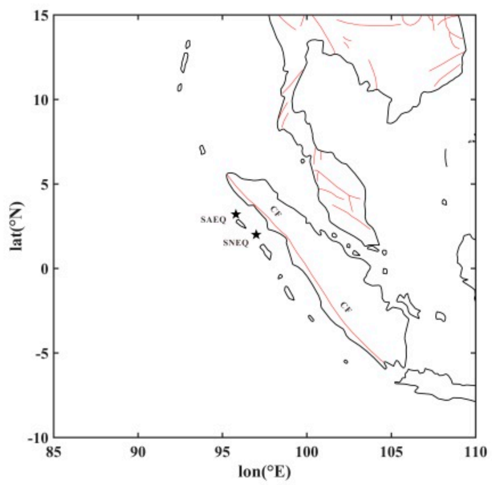

Figure 4. *Cont.*

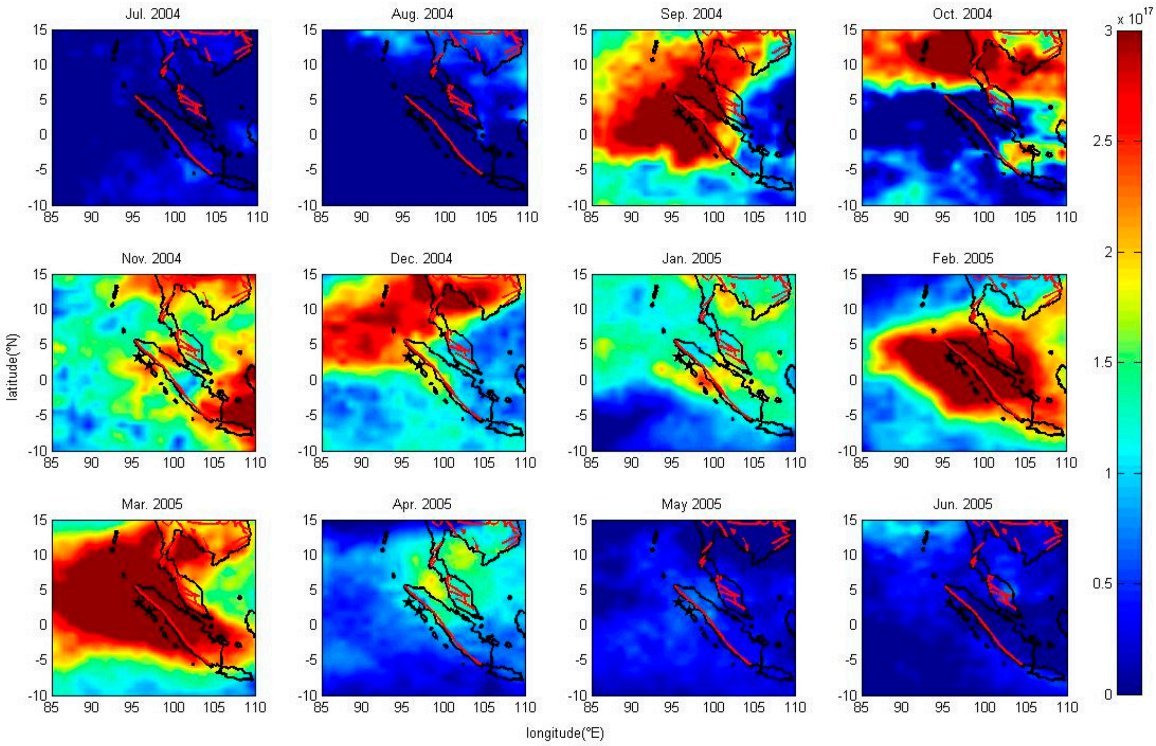

Figure 4. The temporal and spatial variations of TotCO anomaly from July 2004 to June 2005 associated with Sumatra-Andaman M_W 9.1 on 26 December 2004 and Sumatra-Nias M_W 8.6 earthquakes on 28 March 2005. A clean base map with only the epicenter and faults were drawn in order to clearly display the location of the epicenter and faults (the upper figure). Red lines stand for the faults, and black stars mean the epicenters of two great earthquakes (as in Figures 5 and 6). SF refers to Sumatra Fault; SAEQ and SNEQ stand for Sumatra-Andaman Earthquake and Sumatra-Nias Earthquake, respectively.

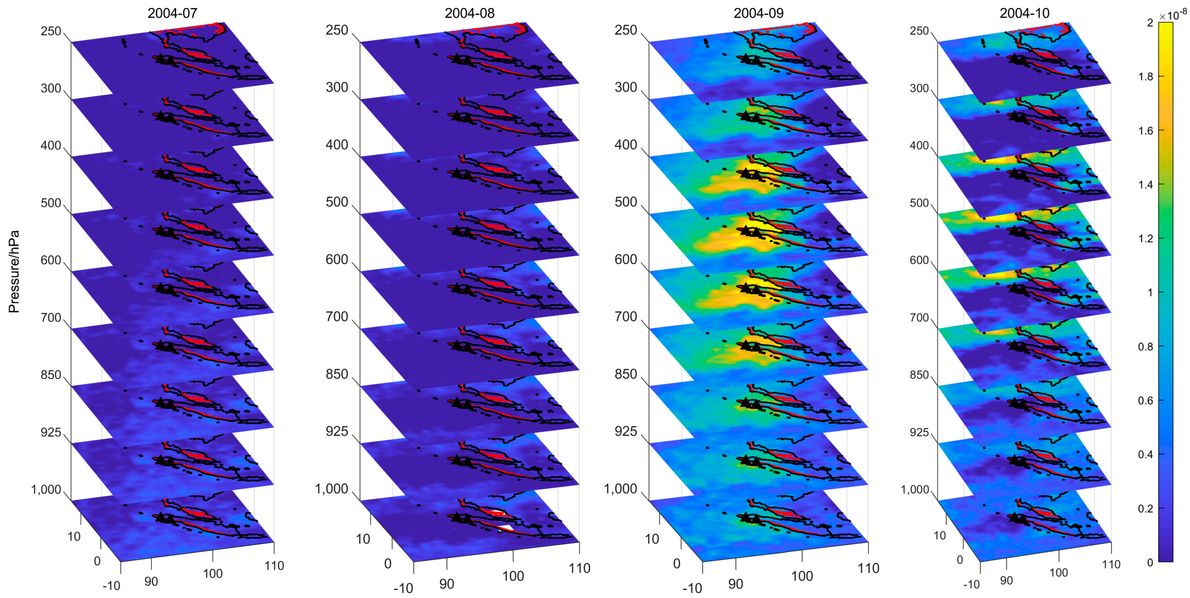

Figure 5. *Cont.*

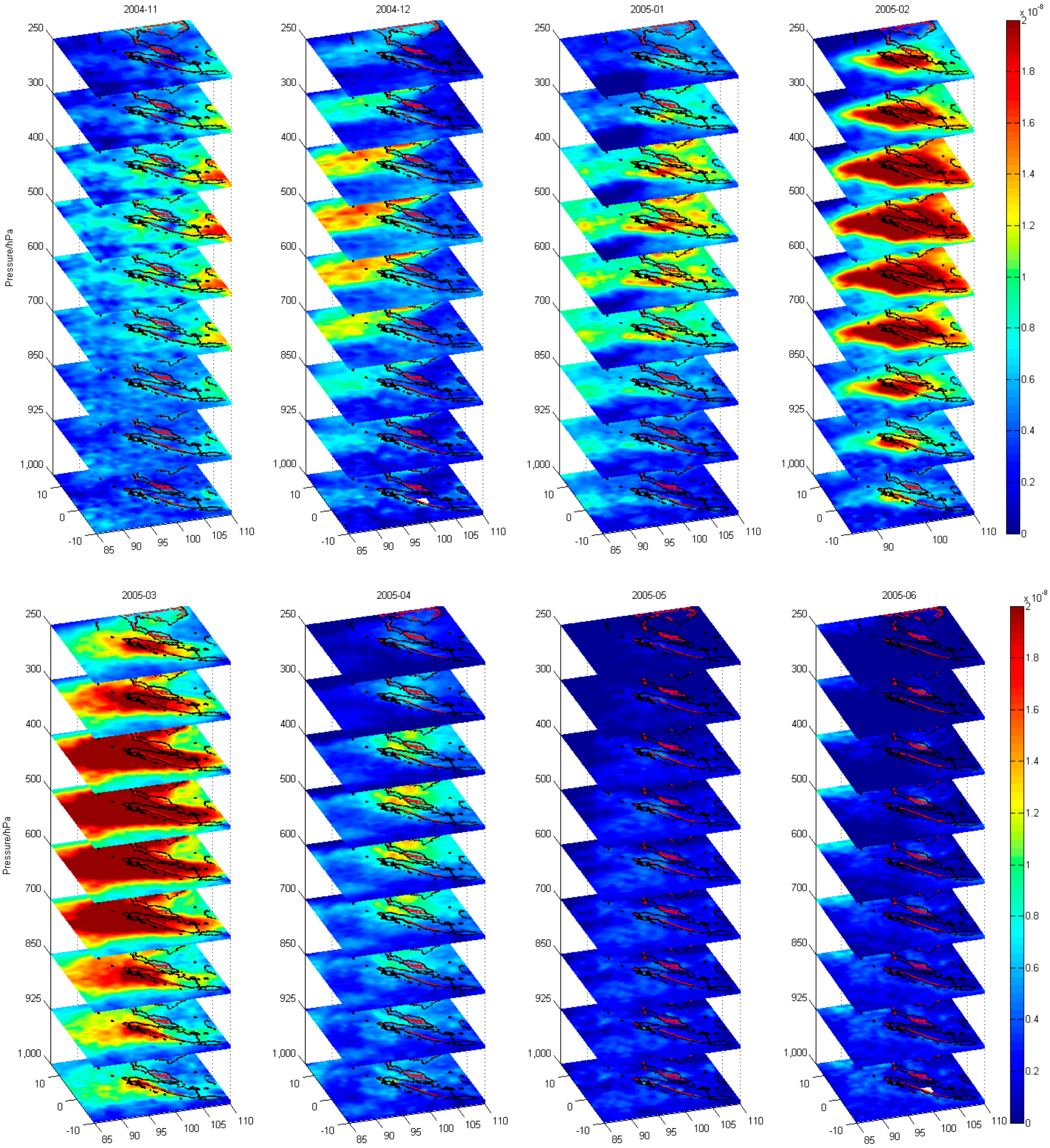

Figure 5. The spatial–vertical variations in CO VMR anomalies in monthly from July 2004 to June 2005 associated with Sumatra-Andaman M_W 9.1 and Sumatra-Nias M_W 8.6 earthquakes [17].

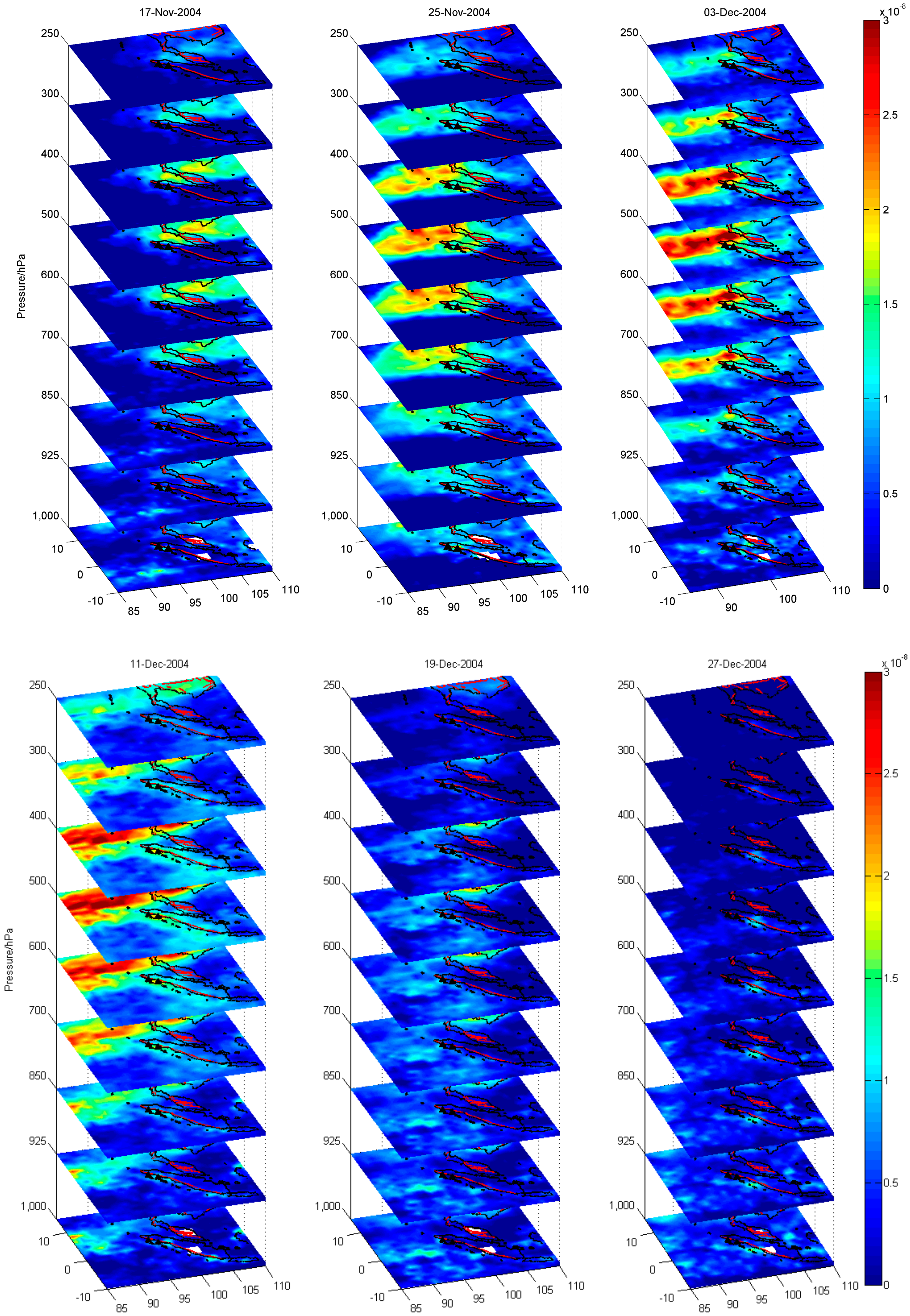

Figure 6. *Cont.*

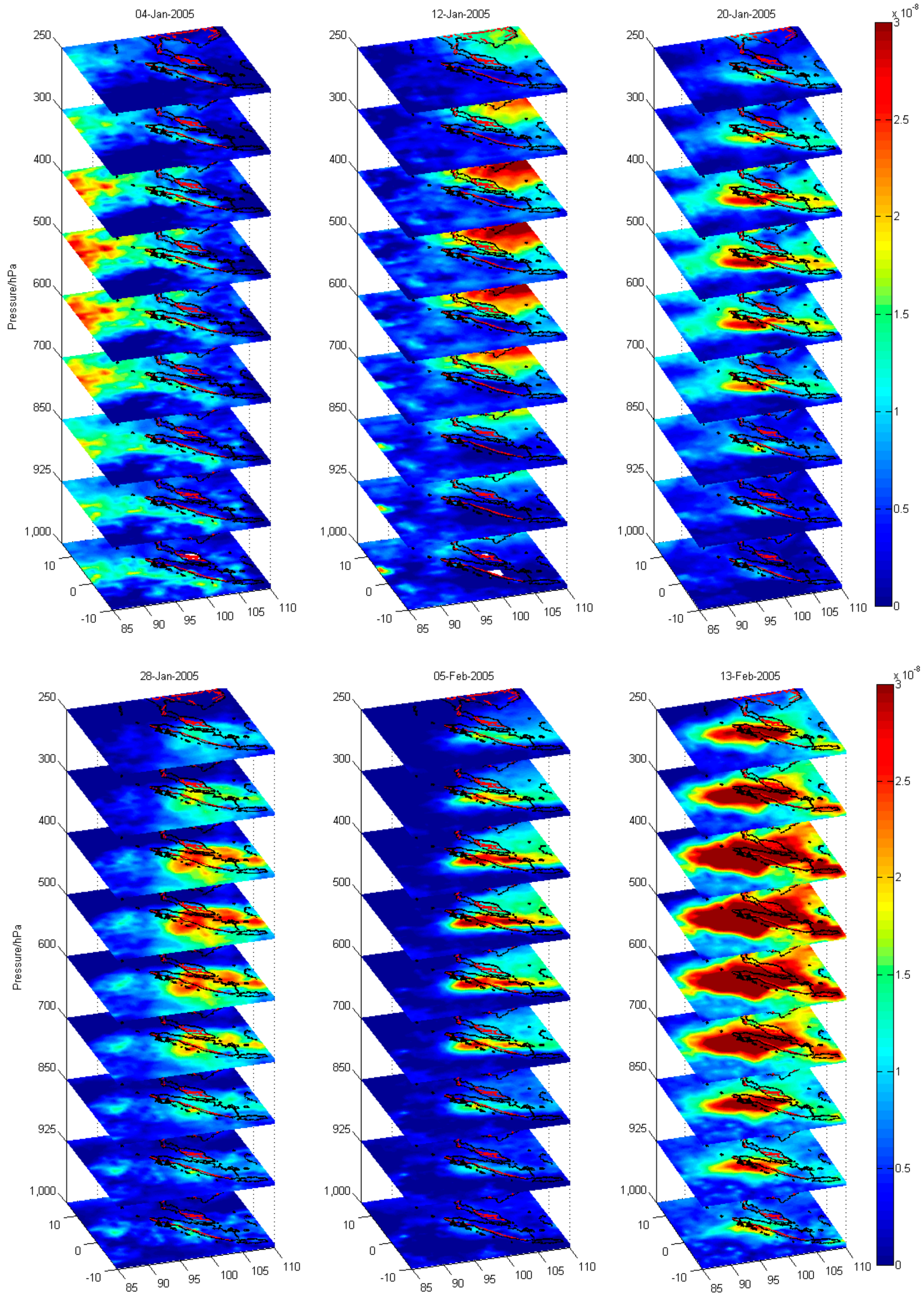

Figure 6. *Cont*.

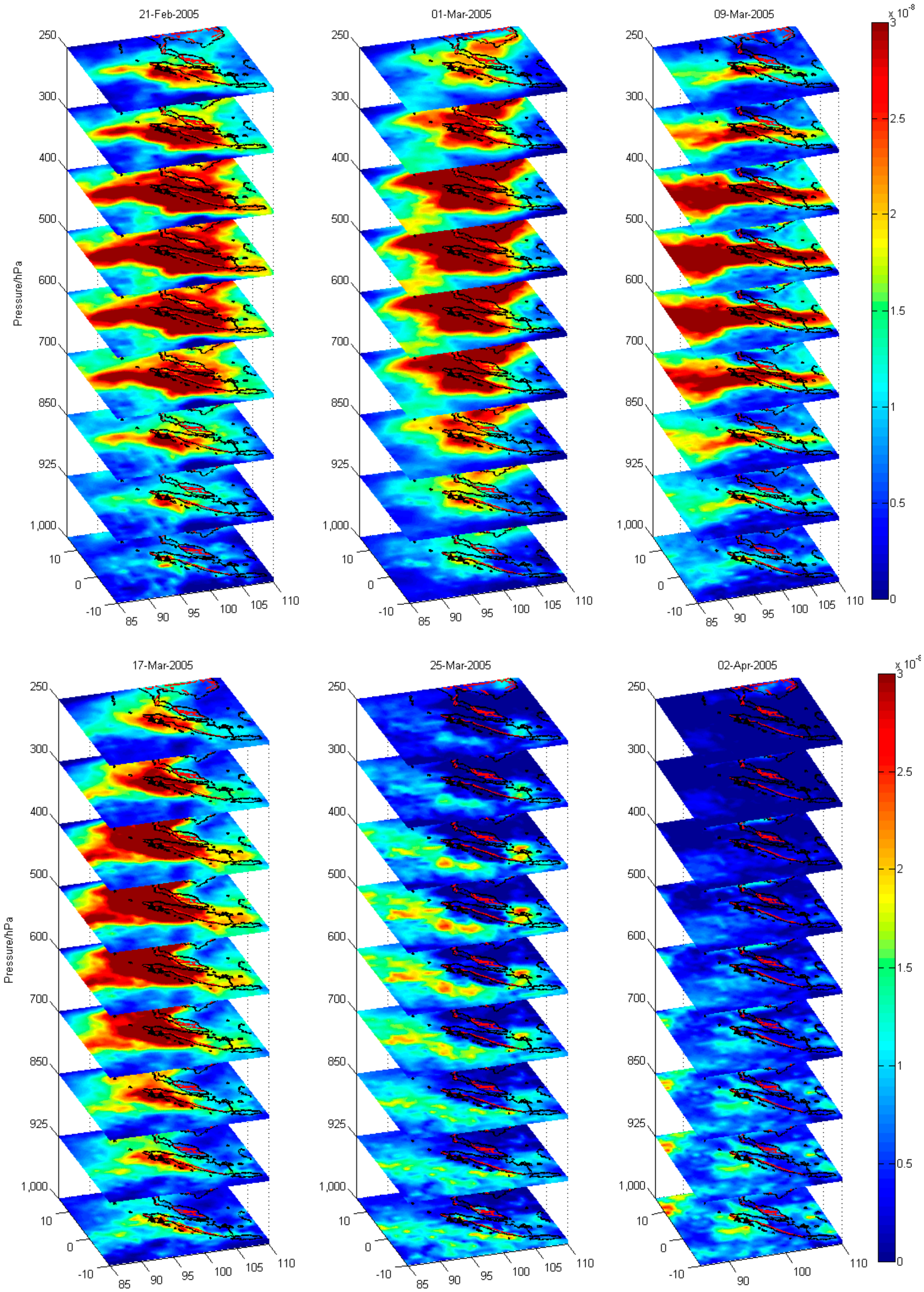

Figure 6. The spatial–vertical variations of CO VMR anomalies in 8-day data from 17 November 2004 to 2 April 2005 associated with Sumatra-Andaman M_W 9.1 and Sumatra-Nias M_W 8.6 earthquakes.

The spatial variations in CO VMR at various altitudes ranging from 1000 to 250 hPa in monthly data are shown in Figure 5 for the period spanning from July 2004 to June 2005. This analysis was conducted for two significant earthquakes: the Sumatra-Andaman M_W 9.1 Earthquake and the Sumatra-Nias M_W 8.6 Earthquake. It was found that elevated CO VMR values were observed over the epicenter area across all layers during September 2004, as well as from January to April 2005. However, the anomalies significantly diminished in April 2005. Despite the AIRS sensor's heightened sensitivity to the troposphere, CO anomalies were more pronounced at altitudes ranging from 400 to 850 hPa compared to the near-surface (925 and 1000 hPa) and higher (250 and 300 hPa) layers. Weak CO anomalies were still found at 925 and 1000 hPa, located near the surface and aligned with the NW-trending Sumatra faults in February and March 2005 (Figure 5).

The spatial–vertical variations in CO VMR in 8-day data from 17 November 2004 to 2 April 2005 (Figure 6) indicated that CO anomalies appeared from 17 November to 11 December 2004, concentrated near the epicenter at 700 and 300 hPa. Subsequently, from 20 January to 17 March 2005, the anomalies were distributed around the epicenter and along the NW Sumatra faults across all layers. These observations indicated a potential link between the CO anomalies appearing in the studied area (Figures 5 and 6) and gas emissions from underground sources during seismic activities.

3.3. CO Variations Associated with Baja California M_W 7.2 Earthquake

The temporal, spatial, and vertical variations in CO anomalies associated with the Baja M_W 7.2 California Earthquake on 4 April 2010 were analyzed based on the monthly TotCO, monthly CO VMR, and 8-day CO VMR data.

The temporal and spatial variations in the TotCO anomaly, as depicted in Figure 7, span from February to May 2010. Notably, the TotCO anomaly appeared in the vicinity of the epicenter area during March, one month prior to the earthquake, and persisted through April, the month in which the earthquake occurred. Specifically, in March, a pronounced pattern of distribution along the San Andreas Fault was observed.

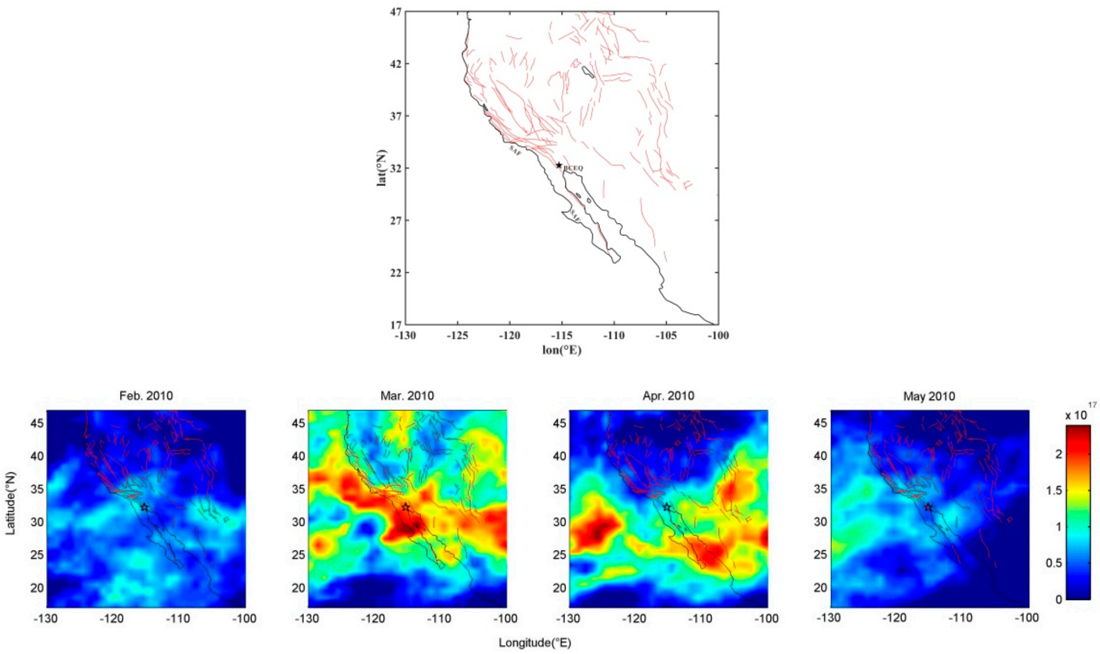

Figure 7. The temporal and spatial variations in TotCO anomaly from February to May 2010 associated with Baja California M_W 7.2 Earthquake. A clean base map with only the epicenter and faults was drawn in order to clearly display the location of the epicenter and faults (the upper figure). The red lines represent the faults and the black star located in the epicenter (as in Figures 8 and 9). SAF refers to the San Andreas Fault and BCEQ stand for Baja California Earthquake.

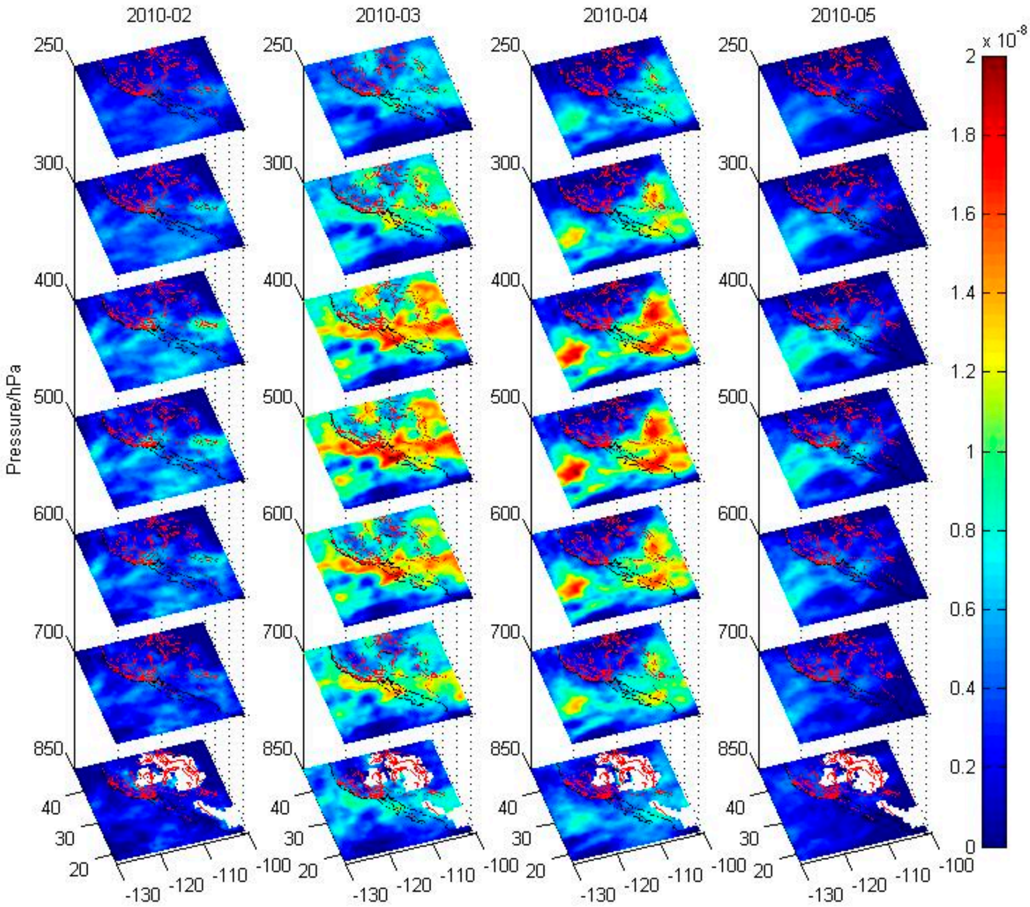

Figure 8. The spatial–vertical variations in CO VMR anomalies in monthly from February to May 2010 associated with Baja California M_W 7.2 Earthquake.

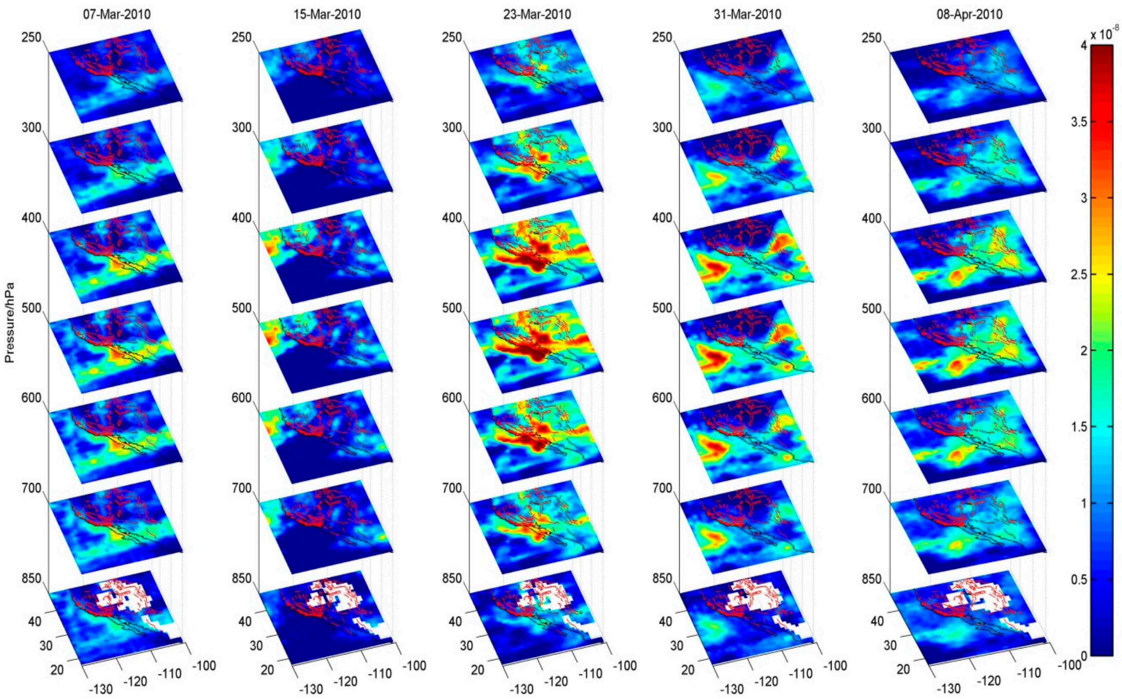

Figure 9. The spatial–vertical variations in CO VMR anomalies in 8-day data from 7 March to 8 April 2010 associated with Baja California M_W 7.2 Earthquake.

Furthermore, Figure 8 shows temporal and spatial variations in CO VMR at altitudes ranging from 850 to 250 hPa in monthly data from February to May 2010 associated with the Baja California Earthquake on 4 April 2010. Elevated CO VMR values were observed over the epicenter area across all layers during March and April of 2010. These observations exhibited a distinct linear feature along the faults, offering further insight into the seismic activity during this period.

Additionally, Figure 9 presents the spatial–vertical variations in CO VMR in 8-day data from 7 March to 8 April 2010. The analysis displayed that CO anomalies mainly emerged on 23 March 2010, specifically concentrated over the epicenter and extending along the fault lines. These anomalies were particularly pronounced at altitudes ranging between 700 and 300 hPa, offering valuable insights into the complex spatial–vertical dynamics of CO VMR during this timeframe.

4. Discussions

The temporal, spatial, and vertical variations observed in CO anomalies exhibited a profound correlation with seismic and tectonic activities. This relationship was particularly evident in the magnitude, rupture length, and the tectonic settings surrounding the epicenter. Furthermore, the type of the fault at which the earthquake occurred also played an important role in these variations in CO anomalies.

The temporal and spatial variations in CO anomalies, presented in both TotCO and CO VMR formats across Figures 1–9 and summarized in Table 1, appear to be strongly influenced by seismic activities. It is notable that concentrations of gases such as CO_2, CO, CH_4, and H_2 are significantly higher in the deeper interiors of the Earth than at atmospheric levels. These underground gases migrate upward along fault zones and fractures that form due to the increasing stress during the generation and occurrence of the earthquakes. This migration is driven by the action of concentration gradients and the fluid pressure, ultimately leading to the release of these gases into the atmosphere [14–17,40]. Therefore, such processes contribute to the elevated CO concentrations observed over the epicenter and along the seismic fault zones (Figures 1–9), as reported by Italiano et al. [41].

The spatial trends in CO anomalies fit well with the fault zones, as depicted in Figures 1–9, also strongly indicating that CO anomalies were closely related to the seismic and tectonic activities. The conclusion is supported by multiple evidence. Firstly, field observations have consistently reported the presence of gas anomalies along fault zones [1,3,42–46]. Secondly, satellite hyper-spectrum data have also proven invaluable in detecting and mapping these anomalies, further corroborating the findings from ground-based observations [14–16,47]. Taking the temporal, spatial, and vertical variations together, these observations provide a comprehensive picture of the spatial and temporal patterns of CO anomalies in relation to seismic and tectonic activities, offering valuable insights into the complex interactions between the Earth's surface and atmosphere.

Table 1. Spatial–temporal features of CO seismic anomalies associated with earthquakes in diverse tectonic environments.

Time	Location	Coordinate	Magnitude M_W	Tectonic Setting	Fault Type	Rupture Length km	Temporal Features			Intensity Max	Spatial Features		Tectonic Illustrations
							Area/km	Time of Occurrence *	Duration		TotCO	CO VMR	
12 May 2008	Wenchuan	31.002°N, 103.322°E	7.9	compressional/internal continental	reverse	~300	100 × 150	−1 w~+1 w	2 w	8 ppb	mass-shaped /strip-shaped	mass-shaped /strip-shaped	Figure 10a [26–28]
26 December 2004	Sumatra-Andaman	3.295°N, 95.982°E	9.1	compressional /subduction/island	thrust and strike-slip	~1200	2000 × 2000	−3 m~+4 m	8 m	30 ppb	mass-shaped	mass-shaped /strip-shaped	Figure 10b [29–31]
4 April 2010	Baja California	32.286°N, 115.295°W	7.2	extensional/sea-land interface	strike-slip	~75	500 × 1500	−1 m~+1 w	5 w	20 ppb	strip-shaped/scatter-shaped	strip-shaped/scatter-shaped	Figure 10c [32–34]

* w and m are the abbreviations for week and month, respectively; "−" and "+" represent pre- and post-earthquake, respectively.

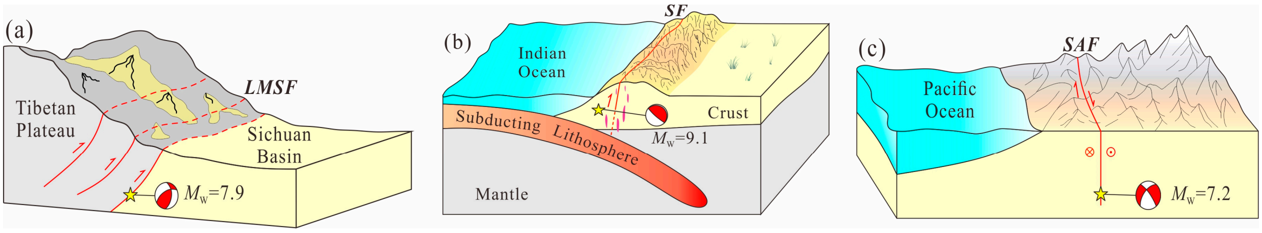

Figure 10. Simplified illustrations showing the tectonic background with the major features and fault types for Wenchuan (**a**), Sumatra-Andaman (**b**), and Baja California (**c**) earthquakes. These diagrams offer a concise visual representation of the tectonic settings and fault mechanisms associated with each seismic event.

Satellite observations reveal a correlation between CO emissions and the three types of earthquakes that occurred in distinct geographical regions. (1) Firstly, the amount of CO released is directly related to both the magnitude of the earthquake and the extent of rupture caused by earthquake. Therefore, the Sumatra-Andaman M_W 9.1 Earthquake, which had the largest magnitude and the longest rupture, resulted in the largest area, strongest intensity, and longest duration of CO anomalies (clearly visible in Figures 4–6 and outlined in Table 1). In contrast, the Baja California M_W 7.2 Earthquake and the Wenchuan M_W 7.9 Earthquake were associated with comparatively lesser anomalies (depicted in Figures 1–3 and 7–9, respectively, and detailed in Table 1). Interestingly, despite its smaller magnitude, the Baja California M_W 7.2 Earthquake exhibited a surprisingly stronger abnormal intensity of CO than the Wenchuan Earthquake, possibly due to its longer rupture length. (2) Secondly, the amount of CO released is closely related to the tectonic settings surrounding the location of the earthquake epicenter. The extensional tectonic setting provides pathways (such as fractures) for gas migration, while the compressional tectonic setting creates overlapping structures that inhibit the rise of deep gases [7,43,46]. This explains why the Baja California Earthquake, despite having the smallest magnitude, exhibited a stronger abnormal intensity of CO compared to the Wenchuan Earthquake (as outlined in Table 1). (3) Thirdly, the amount of CO released is correlated with the specific type of fault where the earthquake occurred. Activities of the strike-slipping faults under tectonic stress might be conducive to the release of underground gases compared to thrust faults (Figure 11, [43,46–49]). From the schematic model, it can be seen that the compression channel present within the thrust fault, when subjected to stress, serves to mitigate the propagation of cracks. This explains why the abnormal intensity of CO associated with the Wenchuan Earthquake was the weakest among the three events examined.

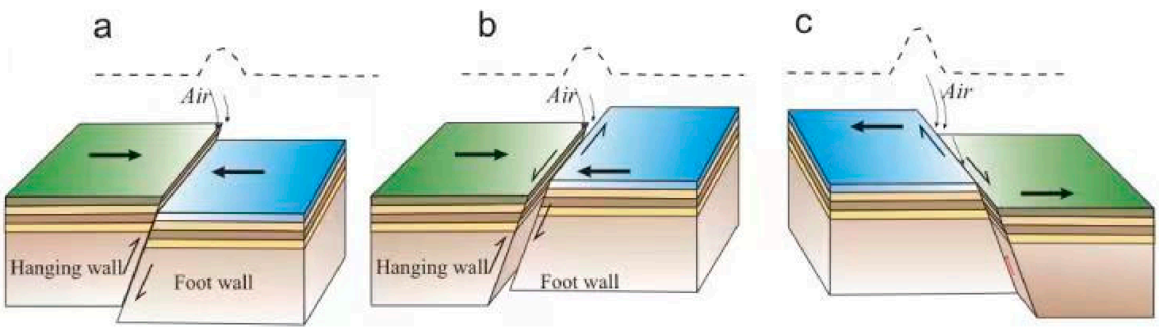

Figure 11. Schematic model showing stress field related to CO degassing in a thrust fault (**a**), thrust and strike-slip fault (**b**), and strike-slip fault (**c**).

CO VMR variations provide better insights than TotCO variations in reflecting anomaly heights and enhancing the accuracy of earthquake anomaly assessments. In the aforementioned earthquake cases, although CO anomalies proximal to the epicenter were detected both before and after the earthquakes (Figures 1, 4 and 7), their direct association with the seismic event was ambiguous. However, the utilization of CO VMR variations (Figures 2, 3, 5, 6, 8 and 9) provided a clearer picture of the journey of CO from the surface to the upper atmosphere following its release. This comprehensive viewpoint greatly strengthened the evidence linking these anomalies to seismic activities and structures, thereby enhancing our understanding of the complex relationship between them.

In summary, these findings highlight the complex interplay between earthquake dynamics, fault type, and CO emissions, offering valuable insights into the Earth's geochemical processes.

5. Conclusions

To uncover the potential relationship between CO anomalies and seismic activities, a comprehensive analysis was conducted on the three-dimensional spatial and temporal variations in CO using AIRS data linked to three distinct earthquakes: the 2008 Wenchuan M_W 7.9 Earthquake in China, the 2004 Sumatra-Andaman M_W 9.1 Earthquake in Indonesia, and the 2010 Baja California M_W 7.2 Earthquake in Mexico. These earthquakes occurred in various geographical regions, exhibiting unique characteristics.

The study revealed anomalies in both TotCO and multiple layers of CO VMR over the epicenters and along the fault zones for all three events. These anomalies were observed both before and after the earthquakes, strongly suggesting a close relationship between CO variations and seismic activity, as well as tectonic structure. This association was most conspicuous in relation to the earthquake magnitude, rupture length, and the tectonic settings surrounding the epicenter. Moreover, the specific characteristics of the fault where the earthquake occurred also emerged as a crucial factor influencing these variations in CO anomalies.

To expand upon the study's findings, future research could explore the mechanisms underlying the observed CO anomalies and their relationship with seismic activity; for example, an investigation of the chemical and physical processes that lead to CO variations in the atmosphere. Importantly, the findings highlighted that the identification of multi-layer CO VMR anomalies could serve as a valuable tool in earthquake anomaly detection. This adds a new dimension to our understanding of the complex interactions between atmospheric chemistry and seismic activity, potentially enhancing earthquake monitoring and prediction capabilities.

Author Contributions: Y.C. conceived the experiments, analyzed the results, and wrote the manuscript. J.H., Z.Z. (Zhaojun Zeng) and Z.Z. (Zhenju Zou) edited and reviewed the manuscript. All authors have read and agreed to the published version of the manuscript.

Funding: This work was supported by the National Key Research and Development Program (no. 2023YFC3012005-1), the National Natural Science Foundation of China (nos. 41403099, 41904092) and IGCP Project 724.

Data Availability Statement: Publicly available datasets were analyzed in this study. This data can be found here: http://disc.sci.gsfc.nasa.gov/ (accessed on 20 December 2021).

Acknowledgments: The authors thank NOAA providing the AIRS products.

Conflicts of Interest: The authors declare no conflict of interest.

References

1. Irwin, W.P.; Barnes, I. Tectonic relations of carbon dioxide discharges and earthquakes. *J. Geophys. Res. Solid Earth.* **1980**, *85*, 3115–3121. [CrossRef]
2. Toutain, J.P.; Baubron, J.C. Gas geochemistry and seismotectonics: A review. *Tectonophysics* **1999**, *304*, 12227. [CrossRef]
3. Chiodini, G.; Cardellini, C.; Amato, A.; Boschi, E.; Ventura, G. Carbon dioxide Earth degassing and seismogenesis in central and southern Italy. *Geophys. Res. Lett.* **2004**, *31*, L07615. [CrossRef]
4. Yang, T.F.; Walia, V.; Chyi, L.L. Variations of soil radon and thoron concentrations in a fault zone and prospective earthquakes in SW Taiwan. *Radiation Measur.* **2005**, *40*, 496–502. [CrossRef]
5. Famin, V.; Nakashima, S.; Boullier, A.; Fujimoto, K.; Hirono, T. Earthquakes produce carbon dioxide in crustal faults. *Earth Planetary Sci. Lett.* **2008**, *265*, 487–497. [CrossRef]

6. Zhou, X.C.; Chen, Z.; Cui, Y.J. Environmental impact of CO_2, Rn, Hg degassing from the rupture zones produced by Wenchuan M_S 8.0 earthquake in western Sichuan, China. *Environ. Geochem. Health* **2015**, *38*, 1067–1068. [CrossRef]
7. Cui, Y.J.; Li, Y.; Si, X.Y.; Yang, L.; Liu, Z.X.; Sun, F.X.; Li, X.Y.; Zheng, H.W.; Du, J.G. Tectonic controls on near-surface variations in CH_4 and CO_2 concentrations along the northwestern margin of the Ordos Block, China. *Geofluids* **2019**, *2019*, 7909483. [CrossRef]
8. Sun, Y.T.; Zhou, X.C.; Du, J.G.; Guo, Z.F. CO diffusive emission in the co-seismic rupture zone of the Wenchuan M_S 8.0 earthquake. *Geochem. J.* **2020**, *54*, 91–104. [CrossRef]
9. Li, Y.; Chen, Z.; Sun, A.H.; Liu, Z.F.; Caracausi, A.; Martinelli, G.; Lu, C. Geochemical features and seismic imaging of the tectonic zone between the Tibetan Plateau and Ordos Block, central northern China. *Chem. Geol.* **2023**, *622*, 121386. [CrossRef]
10. Yang, Y.; Li, Y.; Li, Y.G.; Ji, L.Y.; Gong, Y.; Du, F.; Zhang, L.; Chen, Z. Present-Day Activity of the Anninghe Fault and Zemuhe Fault, Southeastern Tibetan Plateau, Derived from Soil Gas CO_2 Emissions and Locking Degree. *Earth Space Sci.* **2021**, *8*, e2020EA001607. [CrossRef]
11. Tronin, A.A. Remote sensing and earthquakes: A review. *Phys. Chem. Earth Parts A/B/C* **2006**, *31*, 138–142. [CrossRef]
12. Ganguly, N.D. Variation in atmospheric ozone concentration following strong earthquakes. *Int. J. Remote Sens.* **2009**, *30*, 349–356. [CrossRef]
13. Singh, R.P.; Kumar, J.S.; Zlotnicki, J.; Kafatos, M. Satellite detection of carbon monoxide emission prior to the Gujarat earthquake of 26 January 2001. *Appl. Geochem.* **2010**, *25*, 580–585. [CrossRef]
14. Cui, Y.J.; Du, J.G.; Zhang, D.H.; Sun, Y.T. Anomalies of total column CO and O_3 associated with great earthquakes in recent years. *Nat. Hazards Earth Syst. Sci.* **2013**, *13*, 1–7. [CrossRef]
15. Cui, Y.J.; Du, J.G.; Wang, S.M.; Zhang, Y.; Li, X.Y.; Zou, Z.Y.; Jiang, L. Three-Dimensional Variations of Carbon Monoxide Concentration Associated with Wenchuan Earthquake Based on Airs Data. In Proceedings of the IGARSS 2020—2020 IEEE International Geoscience and Remote Sensing Symposium, Waikoloa, HI, USA, 26 September–2 October 2020; pp. 6615–6618.
16. Cui, Y.J.; Ouzounov, D.; Hatzopoulos, N.; Sun, K.; Zou, Z.Y.; Du, J.G. Satellite observation of CH_4 and CO and their abnormal variability associated with Wenchuan M_S 8.0 and Lushan M_S 7.0 earthquakes, in China. *Chem. Geol.* **2017**, *469*, 185–191. [CrossRef]
17. Cui, Y.J.; Zheng, C.; Jiang, L.; Huang, J.N.; Sun, F.X.; Zou, Z.Y.; Du, J.G. Variations of multiple gaseous emissions associated with the great Sumatra earthquakes in 2004 and 2005. *Chem. Geol.* **2023**, *618*, 121311. [CrossRef]
18. Geersen, J.; Scholz, F.; Linke, P.; Schmidt, M.; Lange, D.; Behrmann, J.H.; Volker, D.; Hensen, C. Fault zone controlled seafloor methane seepage in the rupture area of the 2010 Maule earthquake, Central Chile. *Geochem. Geophys. Geosyst.* **2016**, *17*, 4802–4813. [CrossRef]
19. Jing, F.; Singh, R.P.; Shen, X.h. Land-Atmosphere-Meteorological coupling associated with the 2015 Gorkha (M 7.8) and Dolakha (M 7.3) Nepal earthquakes. *Geomat. Nat. Hazards Risk.* **2019**, *10*, 1267–1284. [CrossRef]
20. Jing, F.; Singh, R.P. Changes in Tropospheric Ozone Associated with Strong Earthquakes and Possible Mechanism. *IEEE J. Selected Topics Appl. Earth Obser. Remote Sens.* **2021**, *14*, 5300–5310. [CrossRef]
21. Jing, F.; Singh, R.P. Response of surface and atmospheric parameters associated with the Iran M 7.3 earthquake. *IEEE J. Selected Topics Appl. Earth Obser. Remote Sens.* **2022**, *15*, 3188003. [CrossRef]
22. Liu, Y.J.; Wu, L.X.; Qi, Y.; Ding, Y.F. General features of multi-parameter anomalies of six moderate earthquakes occurred near Zhangbei-Bohai fault in China during the past decades. *Remote Sens. Environ.* **2023**, *295*, 113692. [CrossRef]
23. Guo, G.M.; Cao, Y.G.; Gong, J.M. Monitoring anomaly before earthquake with MODIS and MOPITT data. *Adv. Earth Sci.* **2006**, *2*, 695–698.
24. Cui, Y.J.; Du, J.G.; Zhou, X.C.; Chen, Z.; Li, Y.; Liu, L.; Xie, C.; Zhang, W.B. Geochemical anomaly of CO remote sensing associated with Baja California M_W7.2 earthquake in Mexico. Bulletin of Mineralogy. *Petrol. Geochem.* **2011**, *30*, 458–464.
25. Ma, W.Y.; Zhang, X.D.; Liu, J.; Yao, Y.; Zhou, B.; Yue, C.; Kang, C.L.; Lu, X. Influences of multiple layers of air temperature differences on tidal forces and tectonic stress before, during and after the Jiujiang earthquake. *Remote Sens. Environ.* **2018**, *210*, 159–165.
26. Zhang, P.Z.; Xu, X.W.; Wen, X.Z.; Ran, Y.K. Slip rates and recurrence intervals of the Longmen Shan active fault zone, and tectonic implications for the mechanism of the May l2 Wenchuan earthquake, 2008, Sichuan, China. *Chin. J. Geophys.* **2008**, *51*, 1066–1073.
27. Toda, S.; Lin, J.; Meghraoui, M.; Stein, R.S. 12 May 2008 M = 7.9 Wenchuan, China, earthquake calculated to increase failure stress and seismicity rate on three major fault systems. *Geophys. Res. Lett.* **2008**, *35*, L17305. [CrossRef]
28. de Michele, M.; Raucoules, D.; Lasserre, C.; Pathier, E.; Klinger, Y.; Van Der Woerd, J.; De Sigoyer, J.; Xu, X.W. The M_W 7.9, 12 May 2008 Sichuan earthquake rupture measured by sub-pixel correlation of ALOS PALSAR amplitude images. *Earth Planets Space* **2010**, *62*, 875–879. [CrossRef]
29. Huot, G.; Singh, S.C. Seismic evidence for fluid/gas beneath the Mentawai forearc basin, Central Sumatra. *J. Geophys. Res. Solid Earth.* **2018**, *123*, 957–976. [CrossRef]
30. Lay, T.; Kanamori, H.; Ammon, C.J.; Nettles, M.; Ward, S.N.; Aster, R.C.; Beck, S.L.; Bilek, S.L.; Brudzinski, M.R.; Butler, R.; et al. The great sumatra-andaman earthquake of 26 december 2004. *Science* **2005**, *308*, 1127–1133. [CrossRef]
31. Fujii, Y.; Satake, K.; Watada, S.; Ho, T. Re-examination of Slip Distribution of the 2004 Sumatra–Andaman Earthquake (M_W 9.2) by the Inversion of Tsunami Data Using Green's Functions Corrected for Compressible Seawater Over the Elastic Earth. *Pure Appl. Geophys.* **2021**, *178*, 4777–4796. [CrossRef]
32. Fialko, Y. Interseismic strain accumulation and the earthquake potential on the southern San Andreas fault system. *Nature* **2006**, *441*, 968–971. [CrossRef] [PubMed]

33. Escobar, M.G.; Gallegos-Castillo, C.A.; Arregui-Ojeda, S.M.; Mastache-Román, E.A.; Reyes-Martínez, C.S.; Aladro-Chio, Y.H. Overview of the tectonic and seismicity in Continental Borderland (offshore) Baja California, México. *J. S. Am. Earth Sci.* **2023**, *131*, 104621. [CrossRef]
34. Romero-Andrade, R.; Trejo-Soto, M.E.; Nayak, K.; Hernández-Andrade, D.; Bojorquez-Pacheco, N. Lineament analysis as a seismic precursor: The El Mayor Cucapah earthquake of April 4, 2010 (M_W 7.2), Baja California, Mexico. *Geodesy Geodyn.* **2023**, *14*, 121–129. [CrossRef]
35. Susskind, J.; Barnet, C.D.; Blaisdell, J.M. Retrieval of atmospheric and surface parameters from AIRS/AMSU/HSB data in the presence of clouds. *IEEE Trans. Geosci. Remote Sens.* **2003**, *41*, 390–409. [CrossRef]
36. Barnet, C.; Datta, S.; Strow, L. Trace gas measurements from the Atmospheric Infrared Sounder (AIRS). In *Optical Remote Sensing, OSA Technical Digest*; OWB2; Optica Publishing Group: Québec, Canada, 2003.
37. McMillan, W.W.; Barnet, C.; Strow, L.; Chahine, M.T.; Mccourt, M.L.; Warner, J.X. Daily global maps of carbon monoxide from NASA's Atmospheric Infrared Sounder. *Geophys. Res. Lett.* **2005**, *32*, L11801. [CrossRef]
38. Wu, L.; Qin, K.; Liu, S. GEOSS-Based Thermal Parameters Analysis for Earthquake Anomaly Recognition. *Proc. IEEE* **2012**, *100*, 2891–2907. [CrossRef]
39. Qin, K.; Wu, L.X.; Zheng, S.; Liu, S.J. A Deviation-Time-Space-Thermal (DTS-T) Method for Global Earth Observation System of Systems (GEOSS)-Based Earthquake Anomaly Recognition: Criterions and Quantify Indices. *Remote Sens.* **2013**, *5*, 5143–5151. [CrossRef]
40. Gold, T. Terrestrial sources of carbon and earthquake outgassing. *J. Petrol. Geol.* **1979**, *1*, 3–19. [CrossRef]
41. Italiano, F.; Martinelli, G.; Plescia, P. CO_2 Degassing over Seismic areas: The Role of Mechanochemical Production at the Study Case of Central Apennines. *Pure Appl. Geophys.* **2008**, *165*, 75–94. [CrossRef]
42. Uysal, I.T.; Feng, Y.X.; Zhao, J.X.; Isik, V.; Nuriel, P.; Golding, S.D. Hydrothermal CO_2 degassing in seismically active zones during the late Quaternary. *Chem. Geol.* **2009**, *265*, 442–454. [CrossRef]
43. Van Der Meer, D.G.; Zeebe, R.E.; Van Hinsbergen, D.J.J.; Sluijs, A.; Spakman, W.; Torsvik, T.H. Plate tectonic controls on atmospheric CO_2 levels since the Triassic. *Proc. Natl. Acad. Sci. USA* **2014**, *111*, 4380–4385. [CrossRef]
44. Dupré, S.; Scalabrin, C.; Grall, C.; Augustin, J.-M.; Henry, P.; Şengör, A.M.C.; Görür, N.; Çağatay, M.N.; Géli, L. Tectonic and sedimentary controls on widespread gas emissions in the sea of marmara: Results from systematic, shipborne multibeam echo sounder water column imaging. *J. Geophys. Res. Solid Earth* **2015**, *120*, 2891–2912. [CrossRef]
45. Fu, C.C.; Yang, T.F.; Chen, C.H.; Lee, L.C.; Wu, Y.M.; Liu, T.K.; Walia, V.; Kumar, A.; Lai, T.H. Spatial and temporal anomalies of soil gas in northern Taiwan and its tectonic and seismic implications. *J. Asian Earth Sci.* **2017**, *149*, 64–77. [CrossRef]
46. Tamburello, G.; Pondrelli, S.; Chiodini, G.; Rouwet, D. Global-scale control of extensional tectonics on CO_2 earth degassing. *Nat. Commun.* **2018**, *9*, 4608. [CrossRef]
47. Cui, J.; Shen, X.; Zhang, J.; Ma, W.; Chu, W. Analysis of spatiotemporal variations in middle-tropospheric to upper-tropospheric methane during the Wenchuan M_S = 8.0 earthquake by three indices. *Nat. Hazards Earth Syst. Sci.* **2019**, *19*, 2841–2854. [CrossRef]
48. Sibson, R.H. Structural permeability of fluid-driven fault-fracture meshes. *J. Struct. Geol.* **1996**, *18*, 1031–1042. [CrossRef]
49. Sun, Y.T.; Zhou, X.C.; Zheng, G.D.; Li, J.; Shi, H.Y.; Guo, Z.F.; Du, J.G. Carbon monoxide degassing from seismic fault zones in the Basin and Range province, west of Beijing, China. *J. Asian Earth Sci.* **2017**, *149*, 41–48. [CrossRef]